Crystal Structure of *Methanobacterium thermoautotrophicum* Phosphoribosyl-AMP Cyclohydrolase HisI[†,‡]

J. Sivaraman,[||,§,¶,+] Rebecca S. Myers,[⊥] Lorena Boju,[||,§] Traian Sulea,[||] Miroslaw Cygler,[||,§,¶] V. Jo Davisson,[⊥] and Joseph D. Schrag*[,||,§]

Biotechnology Research Institute, National Research Council, Montreal, Quebec H4P 2R2, Canada, Montreal Joint Center for Structural Biology, Montreal, Quebec H4P 2R2, Canada, Department of Biochemistry, McGill University, Montreal, Quebec, Canada, and Department of Medicinal Chemistry and Molecular Pharmacology, Purdue University, West Lafayette, Indiana 47907

Received March 14, 2005; Revised Manuscript Received June 1, 2005

ABSTRACT: The metabolic pathway for histidine biosynthesis is interesting from an evolutionary perspective because of the diversity of gene organizations and protein structures involved. Hydrolysis of phosphoribosyl-AMP, the third step in the histidine biosynthetic pathway, is carried out by PR-AMP cyclohydrolase, the product of the *hisI* gene. The three-dimensional structure of PR-AMP cyclohydrolase from *Methanobacterium thermoautotrophicum* was solved and refined to 1.7 Å resolution. The enzyme is a homodimer. The position of the Zn^{2+}-binding site that is essential for catalysis was inferred from the positions of bound Cd^{2+} ions, which were part of the crystallization medium. These metal binding sites include three cysteine ligands, two from one monomer and the third from the second monomer. The enzyme remains active when Cd^{2+} is substituted for Zn^{2+}. The likely binding site for Mg^{2+}, also necessary for activity in a homologous cyclohydrolase, was also inferred from Cd^{2+} positions and is comprised of aspartic acid side chains. The putative substrate-binding cleft is formed at the interface between the two monomers of the dimer. This fact, combined with the localization of the Zn^{2+}-binding site, indicates that the enzyme is an obligate dimer.

Histidine biosynthesis is linked to nitrogen metabolism at the level of both precursors and intermediates in the pathway, and histidine is the only amino acid that derives part of its structural carbon from a nucleotide (*1*). In the biosynthetic pathway, ATP is utilized as a substrate and, following ribosylation of the N^1-position and dephosphorylation, the resultant N^1-phosphoribosyl-AMP (PR-AMP)[1] undergoes a ring opening reaction catalyzed by PR-AMP cyclohydrolase coded by the *hisI* gene (Figure 1). This overall transformation renders a carbon and nitrogen from AMP available for the subsequent incorporation into the imidazole ring of histidine.

While its role in histidine metabolism has been known for many years, the PR-AMP cyclohydrolase chemistry draws mechanistic analogies to the general class of purine/pyrimidine deaminases. The PR-AMP cyclohydrolase hydrolyzes the adenine ring of phosphoribosyl-AMP between N^1 and C^6 (Figure 1), while for enzymes such as adenosine deaminase, the hydrolysis releases ammonia. Enzymes such as adenosine deaminase are characterized by using zinc-activated water to effect a nucleophilic attack. Previous studies of the PR-AMP cyclohydrolase have confirmed that its native function requires a zinc ion and classified the protein as a metalloenzyme (*2*). Despite the similarity in the overall reactions, the ligands and coordination of the catalytic zinc vary among the deaminases, making the overall mechanistic comparisons between PR-AMP cyclohydrolases ambiguous. For instance, in adenine deaminase, the catalytic zinc is stabilized by three histidines and an aspartic acid in an octahedral coordination (*3*), metal ligands in cytidine deaminase consist of three cysteines in a tetrahedral coordination (*4*), and in yeast cytosine deaminase, the catalytic zinc is bound by two cysteines and a histidine (*5*).

Histidine biosynthesis is one of the most interesting metabolic pathways from an evolutionary perspective because of the diversity of gene organizations and protein structures. An example of this diversity can be seen in the gene structure of *hisI*. In many species, the gene exists as a fusion with *hisE*. Yet, there are cases among protobacteria and archaea where each gene is expressed as a monofunctional protein, prompting the overall proposal that *hisI* and *hisE* began as separate genes that underwent fusion in later branches of evolution (*6*). Comparison of DNA sequences of the *hisI* genes from the eukaryote *Saccharomyces cer-*

[†] Funding from CIHR Grant 200103GSP-90094-GMX-CFAA-19924 (to M.C.), the National Institutes of Health Grant GM067915 (to V.J.D.), and funding of the Ontario Center for Structural Proteomics from the Ontario Research and Development Challenge Fund is gratefully acknowledged.

[‡] Coordinates and structure factors have been deposited in the Protein Data Bank with code 1ZPS.

* Corresponding author: Dr. Joseph D. Schrag, Biotechnology Research Institute, National Research Council, 6100 Royalmount Avenue, Montreal, Quebec H4P 2R2, Canada. E-mail, Joe.Schrag@nrc-cnrc.gc.ca; tel, (514)496-2557; fax, (514)496-5143.

[||] Biotechnology Research Institute, National Research Council.

[§] Montreal Joint Center for Structural Biology.

[¶] McGill University.

[⊥] Purdue University.

[+] Current address: Department of Biological Sciences, National University of Singapore, Singapore.

[1] Abbreviations: PR-AMP, N^1-(5′-phosphoribosyl)adenosine 5′-monophosphate; TCEP, tris(2-carboxyethyl)phosphine; EDTA, (ethylene-diamine) tetraacetic acid.

10.1021/bi050472w CCC: $30.25
Published on Web 07/07/2005

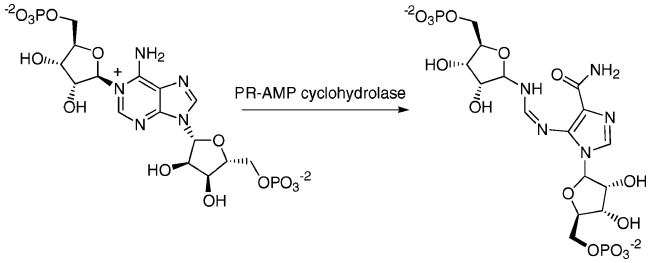

FIGURE 1: Reaction catalyzed by phosphoribosyl-AMP cyclohydrolase HisI.

evisiae, the archaebacterium *Methanococcus vannielii*, and the eubacterium *Escherichia coli* indicates that these genes are derived from a common ancestor; 27% of all nucleotides are identical across the three species with conservation of amino acids at 39% (*7*). These observations suggest that the HisI function in the histidine biosynthetic pathway may have developed prior to the divergence of these biological kingdoms. However, neither a mechanistic consequence regarding the HisI function nor its relationship with other deaminases is apparent from these comparisons.

Biochemical characterization of the PR-AMP cyclohydrolase from *M. vannielii* (*2*) demonstrated the importance of both Zn^{2+} and Mg^{2+} metals in the catalytic mechanism. The presence of Zn^{2+} in the lysis buffer enhances the specific activity and stability of the enzyme, and 1 equiv of bound Zn^{2+} could be removed only by extensive dialysis with 1,10-phenanthroline. We have proposed that a unique sequence motif, $C^{93}(X)_{15}C^{109}H^{110}(X)_5C^{116}$, represents the Zn^{2+} binding domain (*2*). Additionally, the *M. vannielii* enzyme was reversibly inhibited by inclusion of EDTA in the assay mixture, demonstrating that Mg^{2+} is also required for catalytic activity. The consensus sequence motif S^{67}R[S/T]-RXX[L/I]WXKG[E/A]TSG^{81} was suggested to constitute a "P-loop type" region associated with Mg^{2+} and phosphate binding (*2*).

We report here the crystal structure of the phosphoribosyl cyclohydrolase, HisI, from the archaea *Methanobacterium thermoautotrophicum*. Analysis of the three-dimensional structure in light of the biochemical characterization of the homologous *M. vannielii* enzyme identifies the active site and the likely Zn^{2+}- and Mg^{2+}-binding sites. The location of these sites implies that dimerization is required for HisI function and that a functional relationship exists between the active sites of the PR-AMP cyclohydrolase and cytosine deaminase.

MATERIAL AND METHODS

Materials. With the exception of the substrate PR-AMP, all chemicals and buffers were purchased from commercial sources. Synthesis of PR-AMP was performed as previously described (*2*).

Cloning. A pET15b plasmid, MT245, harboring the *M. thermoautotrophicum hisI* gene was kindly provided by the Ontario Center for Structural Proteomics, University of Toronto. The His_6-tagged protein produced from this vector consistently aggregated during purification. The gene was excised from the plasmid using BamHI and NdeI and was inserted into a pET11a vector (Novagen, Darmstedt, Germany) lacking a His tag. *E. coli* MC1061 cells were transformed with the resulting plasmid, pLB1. PCR screening identified colonies containing the insert. The plasmid was purified from one colony designated pLB1-2 and was used to transform *E. coli* BL21(DE3) Gold Magik cells. Cells were plated on Luria−Bertani (LB) plates containing kanamycin and ampicillin. A glycerol stock was prepared from a single colony after a 15 h culture at 37 °C in 5 mL of LB medium.

Expression and Purification. A 50 mL *E. coli* culture prepared from a glycerol stock was incubated overnight at 37 °C and then transferred to 1 L of Circle Grow medium (Bio 101, Inc., Carlsbad, CA) containing ampicillin (0.05 mg/mL) and kanamycin (0.1 mg/mL). After 2 h of growth to an $OD_{600\ nm}$ of 0.9, the production of the enzyme was induced by the addition of IPTG to a final concentration of 1 mM. The culture was incubated for 20 h at room temperature with shaking (250 rpm). Cells were harvested by centrifugation at 4000*g* for 20 min. The cells were lysed by sonication in lysis buffer containing 50 mM Tris-HCl (pH 7.5), 0.5 M NaCl, 0.5 mM $ZnCl_2$, 0.1% (w/v) Triton X-100, 5% (w/v) glycerol, 20 mM β-mercaptoethanol (BME), and one tablet of CompleteC-EDTA free protease inhibitors (Pharmacia, Piscataway, NJ). The cell lysate was cleared by centrifugation (150 000*g*, 30 min, 4 °C), heated to 85 °C for 15 min with gentle agitation, and centrifuged at 3000*g* for 20 min to remove precipitated protein. The supernatant was loaded onto a Mono Q HR 5/5 column (Pharmacia, Piscataway, NJ) equilibrated with 50 mM Tris-HCl (pH 7.5) and 5 mM β-mercaptoethanol and washed with 10 column volumes of equilibration buffer. Protein was eluted with a 20 column volumes linear gradient from 0 to 0.6 M NaCl in 50 mM Tris-HCl, pH 7.5. HisI-containing fractions were pooled, and the protein was dialyzed against 50 mM Tris-HCl (pH 7.5), 200 mM NaCl, 0.5 mM $ZnCl_2$, and 5 mM β-mercaptoethanol. The dialyzed protein was concentrated to 10 mg/mL using a Centricon YM-30 ultrafiltration unit (Millipore, Bellerica, MA) and was stored at 4 °C.

Dynamic Light Scattering. Dynamic light scattering measurements were performed at room temperature on a DynaPro-801 (Protein Solutions, Charlottesville, VA) instrument. The sample was filtered through a 100 μm filter for analysis.

Crystallization. Crystallization experiments were carried out at room temperature using the hanging-drop, vapor-diffusion method. Initial crystallization screening was performed using the Hampton Research (Laguna Niguel, CA) sparse-matrix screens I and II. After optimization of crystallization conditions, the best crystals were produced by mixing the protein solution at a concentration of 2 mg/mL in a 1:1 ratio with a reservoir solution containing 100 mM HEPES-HCl (pH 7.5), 50 mM $CdSO_4$, 1.6 M sodium acetate, and 10% (w/v) glycerol.

Single crystals were picked up directly from the drop using nylon loops and were flash-cooled in a N_2 gas cold stream at 100 K (Oxford Cryosystems, Oxford, U.K.). Diffraction data were collected at beamline X8C at the National Synchrotron Light Source, Brookhaven National Laboratory. Data reduction was done using HKL2000 (*8*). The data used for refinement were collected at a wavelength of 1.009 1 Å. A total of 180 frames were collected with an oscillation angle of 1° per frame. Data used for phasing were collected at a wavelength of 1.282 Å, the Zn absorption maximum. Data statistics are reported in Table 1.

Table 1: Data Collection and Refinement Statistics[a]

	phasing $\lambda = 1.282$ Å	refinement[a] $\lambda = 1.0091$ Å
Data Collection		
unit cell		
a (Å)	39.7	39.8
b (Å)	54.3	54.4
c (Å)	117.3	117.4
resolution range (Å)	50.0−1.86	50.0−1.70
wavelength (Å)	1.2823	1.0091
observed hkl	138718	157479
unique hkl	37937	47949(3809)
completeness (%)	91.8	91.3(70.3)
overall $I/\sigma I$	12.9	40.5(5.5)
R_{sym} (%)	4.4	3.3(12.6)
Refinement		
resolution range (Å)		50.0−1.70
R_{free} (%) no. reflections		23.5 (2338)
R_{work} (%) no. reflections		20.7 (45193)
rmsd bond lengths (Å)		0.01
rmsd bond angles (deg)		1.9
mean coordinate error (Å)		0.20
Ramachandran Plot		
favored region (%)		93.0
allowed region (%)		7.0
generously allowed (%)		0.0
disallowed region (%)		0.0
Average *B*-factors (Å2)		
main chain atoms (no. atoms)		24.5 (1010)
side chain atoms (no. atoms)		27.6 (975)
overall protein atoms (no. atoms)		26.1 (1985)
waters (no. atoms)		29.5 (135)
metal ions (no. atoms)		32.1 (19)
acetate ions (no. atoms)		24.9 (20)

[a] Highest resolution shell in () = 1.76−1.70 Å.

Structure Solution and Refinement. X-ray fluorescence measurements indicated the presence of Zn in the crystals flash-cooled directly from the drop. Initial phases were determined by SAD methods from the data collected at the Zn absorption edge using SOLVE/RESOLVE (*9*, *10*). The partial model obtained accounted for 45% of the expected residues. The model was improved by iterative cycles of manual rebuilding using O (*11*), followed by refinement of the model against a higher resolution "native" dataset using CNS (*12*). The model was refined against data with Bijvoet pairs unmerged because a significant anomalous signal was apparent in the "native" data. Refinement included a bulk solvent correction and an anisotropic overall *B*-factor refinement. Noncrystallographic symmetry restraints were employed during the early refinements, but were not used in later stages and for refinement of the final model. No σ cutoff was used during refinement. Validation of the model was done using PROCHECK (*13*).

The identities of the heavy atoms contributing to the anomalous signal were assigned by comparison of peak heights in anomalous differences maps calculated using phases from the refined model. All of the heavy atoms were assigned as Cd^{2+} ions because the relative peak heights in the anomalous maps were identical in maps calculated from data collected at the Zn absorption maximum (1.282 Å, $\Delta f'' = 5.8$) and at the remote wavelength of 1.494 Å, where the Zn anomalous contribution is very low ($\Delta f'' = 0.64$). The Cd^{2+} anomalous contribution, in contrast, is significant at both of these wavelengths ($\Delta f'' = 3.4$ and 4.4, respectively). Assignment as Cd^{2+} is consistent with the high concentration (50 mM) of $CdSO_4$ being essential for crystallization. This interpretation explains why three-wavelength MAD phasing around the Zn absorption edge was unsuccessful. Since all the bound metal ions are Cd^{2+} ions, the data for all three wavelengths contains approximately equal anomalous contributions and there are no differences that contribute to phase information.

Docking of a Tetrahedral Intermediate. A model of 6-OH PR-AMP, a possible transition state in the reaction catalyzed by HisI, was docked into one of the two putative active site clefts of the HisI homodimer. The ligand was first manually positioned in two independent orientations that differed by an approximate 2-fold rotation that relates the two ribose phosphate groups on either end of the substrate's adenine ring. In both orientations, the 6-OH oxygen atom was placed within coordination distance of the Cd^{2+} ion representing the putative catalytic Zn^{2+} ion. Another Cd^{2+} ion that likely represents a bound Mg^{2+} ion, as well as two water molecules buried at the bottom of the binding site cleft, is also retained from the crystal structure.

For each orientation of 6-OH PR-AMP, bound conformations were modeled by a search using a Monte Carlo minimization (MCM) procedure (*14*−*16*). In each MCM cycle, a starting conformation was generated by randomly perturbing one or more dihedral angles of the ligand, with the 6-OH oxygen as an anchor atom. This starting conformation then was subjected to an energy minimization in which the ligand, ions, and water, as well as a predefined set of protein residues extending 8 Å around the ligand, were allowed to relax up to an rms gradient of 0.05 kcal/(mol·Å). Three thousand MCM cycles were carried out to sample six rotatable bonds of the bound ligand (two rotors between the purine moiety and the ribose rings, plus four rotors between the ribose rings and their phosphate groups). The lowest energy ligand conformation was re-docked into the initial (crystallographic) protein geometry followed by an energy minimization in the same binding site region up to an rms gradient of 0.01 kcal/(mol·Å), thus leading to a final model for each binding orientation.

Conjugate gradient energy minimizations were carried using the AMBER all-atom molecular mechanics force field with the PARM94 parameter set for proteins (*17*) and the GAFF parameter set for organic compounds (*18*). A distance dependent ($4r_{ij}$) dielectric and an 8 Å nonbonded cutoff were employed. The protonation state at physiological pH was adopted with the exception of the Zn-chelating Cys residues, which were ionized. Partial atomic charges of 6-OH PR-AMP were obtained by a two-stage-restrained fitting procedure to the single-point HF 6-31G* electrostatic potential (*17*, *19*). AMBER-compatible, charge-delocalized models with tetrahedral and octahedral geometries were used for the Zn^{2+} and Mg^{2+} ions, respectively (*20*). During all energy minimizations, the distance between the 6-OH oxygen atom of the transition state and the Zn^{2+} ion was constrained within the 2.0−2.5 Å range with a harmonic potential of 200 kcal/(mol·Å^2).

PR-AMP Cyclohydrolase Assay and Kinetic Constants. Protein concentrations were determined by total protein amino acid analysis (ΔA_{280}/mg 1.14). The cyclohydrolase assay followed the established procedure (*2*). Briefly, routine assays were conducted at 30 or 65 °C in a UV−vis spectrophotometer monitoring changes in absorbance at 300

nm ($\Delta\epsilon_{300\ nm}$ 6700 M^{-1} cm^{-1}) or 260 nm ($\Delta\epsilon_{260\ nm}$ 8020 M^{-1} cm^{-1}). Each assay contained 50 mM Tris-HCl (pH 7.5), 1 mM EDTA, 5 mM $MgCl_2$, and 50 μM PR-AMP in a total volume of 1 mL. The reaction was initiated by the addition of 0.1−1 μg of PR-AMP cyclohydrolase. Steady-state kinetic constants were determined by varying the concentration of PR-AMP from 5 to 150 μM. The pH rate profiles were carried out in 30 mM Bis-Tris Propane-HCl (pH 6.5, 7.0, 7.5, 8.0, 8.5, 9.0) at 65 °C. Substrate saturation curves at each pH were determined from six substrate concentrations over the range of 2.5−100 μM PR-AMP with observation at 260 nm.

Metal Exchange and Protein−Metal Ion Contents. All buffers used for dilution and desalting of protein samples were prepared in metal-free glassware following treatment with Chelex (*1*, *21*). A 0.5 mL aliquot of *M. thermoautotrophicum* PR-AMP cyclohydrolase prepared as above was dialyzed at 1 mg mL^{-1} against 3× 1 L of 0.1 mM $CdSO_4$ to directly exchange the active site zinc with cadmium. Verification of metal exchange was accomplished by ICP-MS on the sample, measuring both zinc and cadmium. All samples of PR-AMP cyclohydrolases were desalted using Sephacryl S-200 HR MicroSpin columns. Each sample was passed through two MicroSpin columns before dilution into 2% HNO_3. A calibration curve was generated using standard addition of the metal of interest to control against matrix effects. Briefly, an increasing known amount of metal was added to each sample. Each sample was then analyzed by ICP-MS typically using protein at 10 ppb. The resulting values were then plotted in Cartesian fashion, with *x* and *y* coordinates corresponding to the known concentration of added metal versus the ICP-MS measurement for that sample, respectively. The amount of metal in the original sample was determined by the *x*-intercept of this plot. ICP-MS samples were analyzed at the Campus-wide Mass Spectrometry Center at Purdue University.

RESULTS

The molecular weight of the *M. thermoautotrophicum* HisI monomer is 15 458 Da. SDS−PAGE analysis of the purified protein under reducing conditions revealed two bands, one corresponding to a monomer and the other to a dimer. Native-PAGE showed a single band corresponding to a dimer. Consistent with the presence of a dimer, light-scattering studies indicated the presence of a single species with a molecular weight of ∼37 kDa. Although the cysteine residues in the protein are located at the dimer interface, they form metal-binding sites and no intermolecular disulfide bonds are observed. The observation of dimers in the SDS gels is, therefore, not likely to result from intermolecular disulfide bonds.

Crystallization and Phasing. Crystallization of HisI required high concentrations (50 mM) of Cd^{2+} ions. The crystals belong to the orthorhombic space group $P2_12_12_1$, with unit-cell parameters $a = 39.8$, $b = 54.4$, $c = 117.4$ Å. The crystals routinely diffract to 2 Å resolution and the best crystals diffract to 1.7 Å resolution. A dimer constitutes the asymmetric unit, and the solvent content is approximately 40%.

Zinc is required for enzymatic activity of *M. vannielii* PR-AMP cyclohydrolase (*2*) and presumably for all orthologs. We, therefore, included 0.5 mM $ZnCl_2$ throughout the purification and crystallization of *M. thermoautotrophicum* HisI to stabilize the protein. We anticipated that bound Zn atoms would provide a convenient source of phase information. X-ray fluorescence measurements on flash-cooled crystals showed the presence of Zn, and phases were obtained by SAD methods from data collected at the Zn absorption maximum. However, the high concentration of Cd^{2+} in the crystallization solution (50 mM) provided another potential source of anomalous scatterers that could contribute some of the observed bound metal ions. Anomalous difference maps were used to distinguish between potential Cd^{2+} and Zn^{2+} atoms. The peaks observed in anomalous difference maps, calculated from datasets collected at the Zn absorption maximum where the Zn contribution to the anomalous signal is strong and at a remote wavelength, where the anomalous contribution from Zn is very small, are nearly identical (see Materials and Methods for details). This observation suggests that none of the heavy atoms contributing to the anomalous signal are Zn^{2+} ions. All of the metal ions observed in the electron density are, therefore, interpreted as Cd^{2+} ions.

Overall Structure. The asymmetric unit of the crystal comprises a dimer. Chain A of the refined model includes residues 8−131, and chain B includes residues 4−131. The model also includes 19 Cd^{2+} ions, 5 acetate ions and 129 water molecules and has been refined to an *R*-factor of 0.209 and R_{free} of 0.236. The mean temperature factors reported in Table 1 demonstrate that chain B is generally better ordered than is chain A. The N-terminal 20 residues of chain A, in particular, are poorly ordered, and only fragmented electron density is observed for residues 16−21. Electron density for the long side chains (Lys, Arg, Glu) are poorly defined for many residues in chain A. The loop encompassing residues 115−120, however, is better ordered in chain A than in chain B. Data statistics and the quality of the model are indicated in Table 1.

Each monomer is composed of four β-hairpins (Figure 2A). On one side of the monomer, hairpins 1 (residues 23−42) and 3 (residues 76−98) pack in an antiparallel manner, forming a four-stranded mixed β-sheet. Packed against one face of this β-sheet are hairpin 2 (residues 54−69) and the helix that is inserted between hairpins 1 and 2.

The overall dimensions of the dimer in the asymmetric unit of the crystal are 40 × 50 × 53 $Å^3$. The root-mean-square (rms) deviation in the positions of Cα atoms in the two monomers is 0.39 Å. The dimer interface is formed by interactions of hairpins 1, 3, and 4 of each monomer (Figure 2B). The β-sheets formed by hairpins 1 and 3 pack face to face, primarily by interactions of hydrophobic residues, with a large percentage being the branched residues valine, isoleucine, and leucine. Hairpin 4 (residues 111−122) packs against hairpin 3 of the other monomer within the dimer via hydrogen bonding characteristic of parallel β-structure. This domain swapping, in effect, extends the mixed β-sheet from four strands to six strands. The total surface area buried in the dimer interface is ∼3100 $Å^2$, more than 40% of the total molecular surface area of each monomer.

The most conspicuous features of the HisI model are the two surface clefts that are formed at the interface between the two molecules and are related by the dimer 2-fold symmetry (Figure 3A). Four Cd^{2+} ions are bound in each of these surface clefts (Figure 3B). One of these metal ions, $Cd^{2+}(1)$, is coordinated by the side chains of three cysteines.

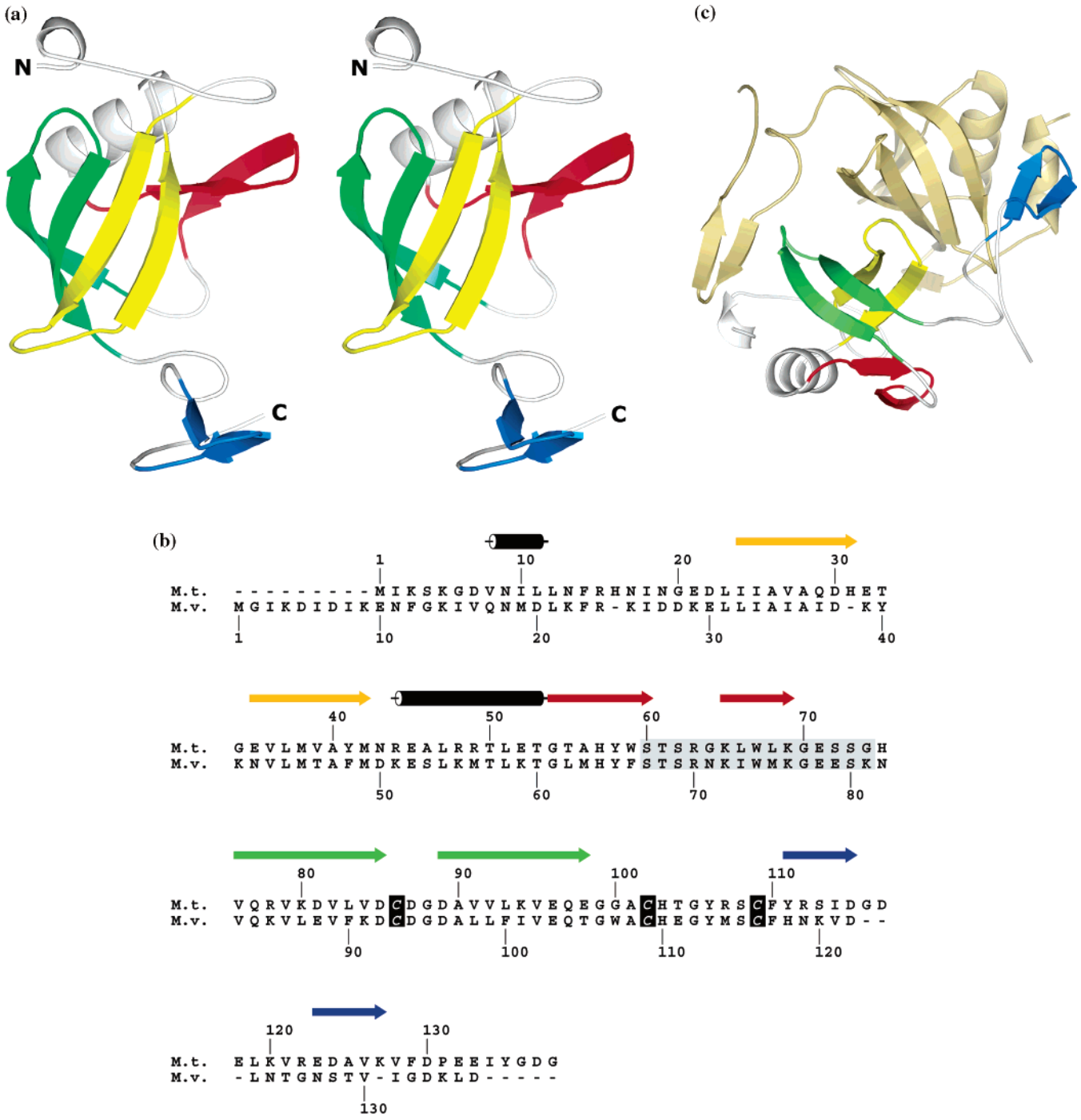

FIGURE 2: Ribbon diagram of HisI. (A) Stereoview of HisI monomer. β-hairpins 1−4 are colored yellow, red, green, and blue, respectively. (B) Sequence alignment of *M. thermoautotrophicum* and *M. vannielii* HisI. Secondary structure observed in the *M. thermoautotrophicum* enzyme is indicated. The β-strands are colored according to the hairpins to which they contribute, with hairpin colors as in panel A. The putative P-loop motif is marked in gray, and the Zn^{2+}-binding cysteine residues are marked in black. This figure was smade using ALSCRIPT (*22*). (C) HisI dimer viewed approximately down the noncrystallographic symmetry axis. Chain A is colored gold, and Chain B is colored as in panel A. Note domain swapping of hairpin 4. This figure was made using PyMol (www.pymol.org).

Cys86 comes from one monomer, whereas Cys102 and Cys109 come from the other monomer. The tetrahedral coordination is completed by the oxygen atom from an acetate molecule or by a water molecule (Figure 3C). Adjacent to these cysteines is a cluster of three aspartic acid residues. The carboxylate oxygen atoms (residues 85, 87, and 89 in the loop between the β-strands of hairpin 3) and several water molecules octahedrally coordinate another cadmium ion, $Cd^{2+}(2)$, bound in the cleft (Figure 3C). A third Cd^{2+} ion is bound between the acidic and cysteine clusters and is coordinated by Asp85 and Cys86 from one monomer, Cys109 from the other monomer, and solvent molecules. The fourth Cd^{2+} ion is bound to residues His16 and Asp89.

Comparisons of 98 amino acid sequences of HisI orthologs from various prokaryotic, archeal, and eukaryotic organisms indicate that HisI was well-conserved during evolution. Invariant residues in all these sequences are Ser60, Lys69, Gly70, Asp87, Cys102, His103, and Cys109. Trp67 is substituted by arginine in the sequence from *Pyrococcus furiosus*, but the alkyls chain of arginine can also make

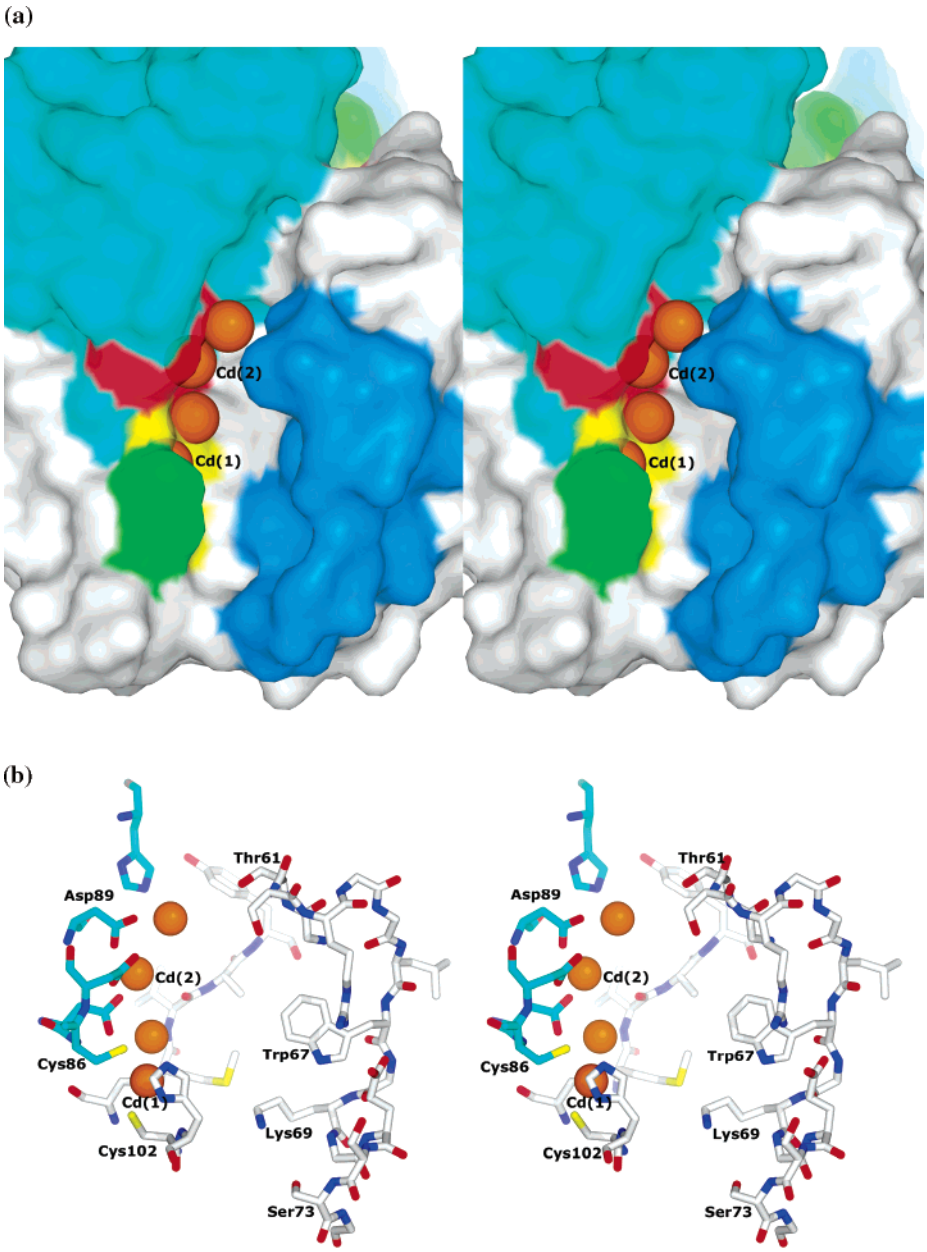

FIGURE 3: CONTINUED

hydrophobic contacts. Asp85, Cys86, and Asp89 are not conserved in the putative HisI sequence from *Leptospira interrogans* (Swiss-Prot entry Q8F8K4), but the catalytic competence of this protein is uncertain. These invariant and highly conserved residues of HisI map to the cleft described above (Figure 3A). Residues 60−70 (one β-strand of hairpin 2) and 102−109 (connection between hairpin 3 and 4) from one monomer are at one end of the cleft, and residues 85−89 (the loop between the two β-strands of hairpin 3) from the other monomer are on the side of the cleft. The conserved residues include the metal ion binding aspartates and cysteines.

We were unable to crystallize HisI in the absence of Cd^{2+}, and even reduction of the Cd^{2+} concentration destabilized the crystals. This requirement reflects the Cd^{2+} ions participating in intermolecular contacts crucial for crystal formation. Two of the most prominent features in electron density maps correspond to the Cd^{2+} ions bound between symmetry related molecules. The first metal atom is coordinated by Glu52B from one dimer and by His103A and Cys86B from the symmetry related dimer. The second is bound by Cys86A and His103B from one dimer and by Glu123B from the symmetry related dimer.

A DALI search using the HisI monomer as a search model identified several similar proteins with *Z* scores ranging from 3.6 to 4.3. The highest score was for the N-terminal β-sandwich domain of the ϵ subunit of the *E. coli* proton-translocating ATP synthase (PDB code: 1E79 (*23*, *24*)). These two domains superimpose with an rms deviation of 2.7 Å for 60 Cα atoms. The ϵ-subunit inhibits the ATPase activity in isolated F1-ATPase and is essential for the coupling of proton translocation to ATP synthesis. The ATP-binding site of the ATPase is, however, far from the ϵ-subunit, and the significance of the structural similarity between HisI and the ATPase subunit is not clear.

HisI is also structurally similar to the N-terminal domain of the *Thermus thermophilus* ribosomal protein TL5 (PDB code 1FEU (*25*)) and to the large subunit ribosomal protein

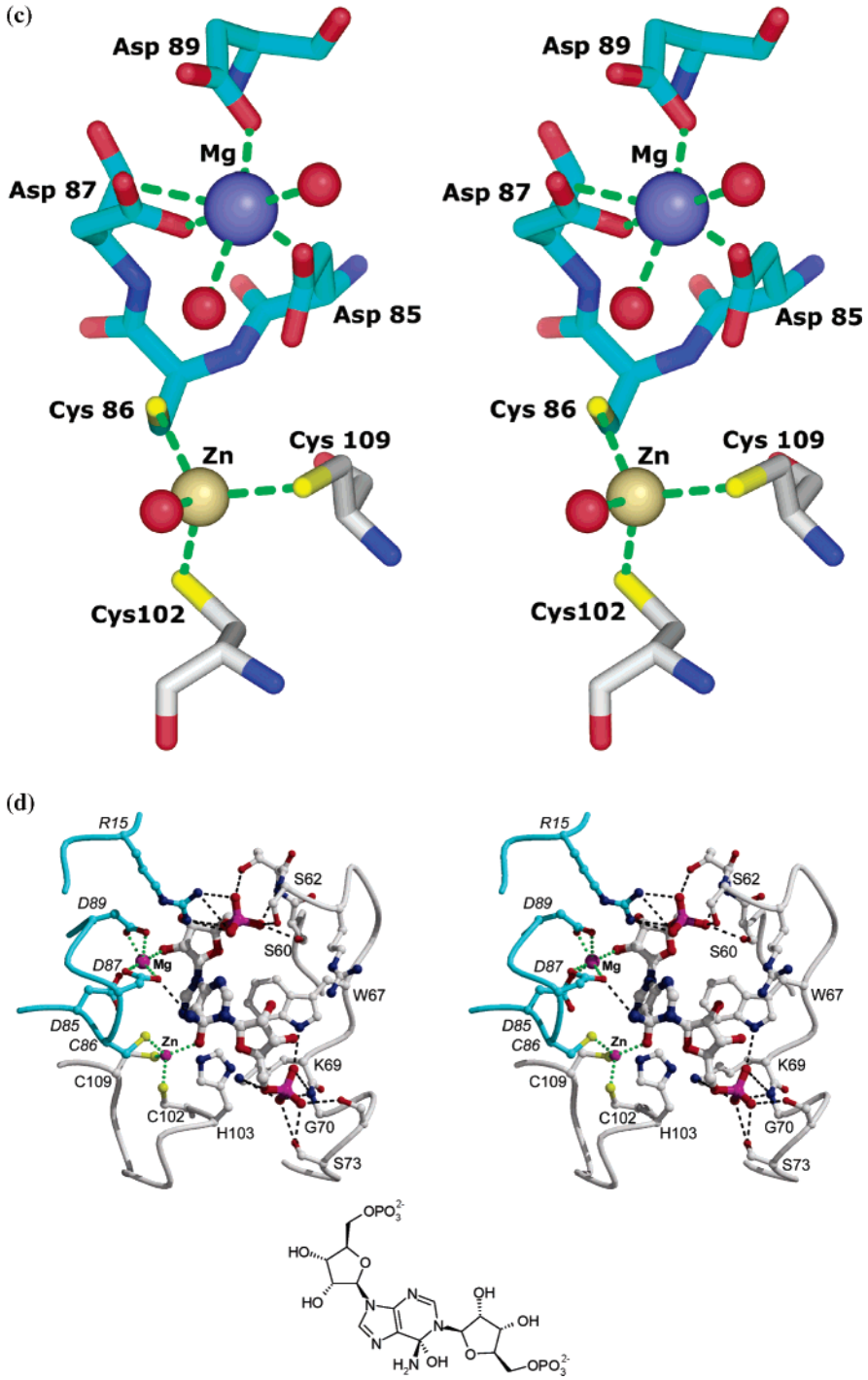

FIGURE 3: (A) Stereoview of the surface of the putative substrate-binding cleft showing the positions of conserved residues and $Cd^{2+}(1)$ and $Cd^{2+}(2)$ ions in the cleft. Residues in cyan derive from chain A, and those in white derive from chain B. Asp and Cys residues in the cleft are red and yellow, respectively. The blue (residues 60−74) and green (H103) residues are residues which are highly conserved in HisI proteins from a wide variety of organisms. (B) Stereoview of the residues forming the cleft at the dimer interface. The oxygens are colored in red, nitrogens in blue, Cd^{2+} in orange, carbons of monomer A in cyan, and those of monomer B in white. (**C**) Coordination of the putative metal binding sites. The site of $Cd^{2+}(1)$ has a tetrahedral coordination and is most likely the Zn^{2+}-binding site (marked Zn in the figure). The site of $Cd^{2+}(2)$ has six ligands and is most likely the Mg^{2+}-binding site (marked Mg in the figure). Water molecules are shown as red spheres. Coloring of atoms in monomers A and B are like in panel B. (D) The lowest energy conformer of the putative transition state of PR-AMP in the cleft. Close-up of the active site of HisI with the model of the transition state bound to the enzyme. Carbon atoms from residues in chain A are in cyan, and those from chain B are white. Hydrogen bonds and metal coordination bonds are represented by black and green dashed lines, respectively. A schematic representation of the putative transition state is also shown.

L25 from *E. coli* (PDB code 1DFU (*26*)). The HisI model superimposes on TL5 with an rms fit of 3.0 Å for 63 Cα atoms and on L25 with an rms fit of 3.3 Å for 58 Cα atoms. TL5 and L25 are functional analogues (*27*), both binding the 5S rRNA. The rRNA-binding site of these proteins is on the face of the molecule that forms the dimer interface in HisI. Therefore, little functional similarity between HisI and TL5/L25 is apparent.

PR-AMP Cyclohydrolase Kinetic Constants and pH Profile. The specific activity of the purified protein was first

Table 2: Specific Activity as a Function of Temperature

	30 °C (μmol/min)/mg	65 °C (μmol/min)/mg
M. vannielii His I	12	35
M. thermoautotrophicum His I	5.3	24

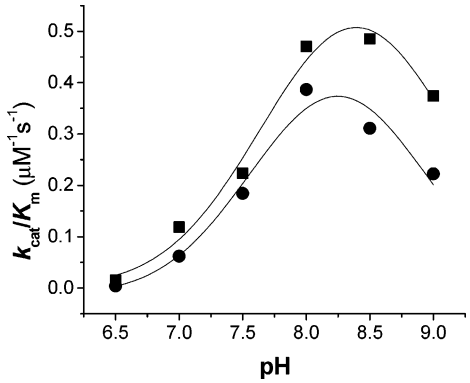

FIGURE 4: pH profile of *M. thermoautotrophicum* PR-AMP cyclohydrolase; ■, zinc-containing protein, pK_a = 7.55; ●, cadmium-containing protein, pK_a = 7.54.

analyzed at 30 °C and pH 7.5 following the protocol established for PR-AMP cyclohydrolase from *M. vannielii.* The measured specific activity (5.3 U/mg) was less than half that of *M. vannielii* PR-AMP cyclohydrolase (12 U/mg). Therefore, the assay was repeated at the optimal growth temperature of *M. thermoautotrophicum* (65 °C). The specific activity at 65 °C was 24 U/mg, compared to 35 U/mg for *M. vannielii* PR-AMP cyclohydrolase (Table 2). The steady-state kinetic constants were determined for *M. thermoautotrophicum* HisI at 65 °C and pH 7.5 using the established protocols (*2*). The resulting constants, $K_m = 14 \pm 3$ μM, $k_{cat} = 8$ s^{-1} ($k_{cat}/K_m = 6 \times 10^5$ M^{-1} s^{-1}) are in good agreement with the constants determined for *M. vannielii* PR-AMP cyclohydrolase (*2*), $K_m = 9.9 \pm 1.7$ μM, $k_{cat} = 4.1 \pm 0.3$ s^{-1} ($k_{cat}/K_m = 4.1 \times 10^5$ M^{-1} s^{-1}). The k_{cat}/K_m pH profile of *M. thermoautotrophicum* HisI indicates a single pK_a at 7.5 ± 0.2 (Figure 4), in good agreement with *M. vannielii* PR-AMP cyclohydrolase (7.3 ± 0.1) (*2*). The greater drop in *M. thermoautotrphicum* activity in the basic range could be due to the difference in the pI between these orthologs (*M. thermoautotrophicum* HisI pI = 5.2, *M. vannielii* HisI pI = 6.3).

Cadmium-Containing PR-AMP Cyclohydrolase Steady-State Kinetic Analysis. The crystal structure of *M. thermoautotrophicum* HisI was solved in the presence of 50 mM cadmium, and consequently, this ion replaced the Zn^{2+} in the active site of this zinc metalloenzyme. To determine if the crystal structure represents the active form of the enzyme, direct metal exchange through extensive dialysis was performed to substitute cadmium for zinc. The metal content of various preparations of the *M. thermoautotrophicum* HisI were analyzed by ICP-MS. Protein samples analyzed after the initial purification from *E. coli* in the presence of 2-mercaptoethanol and $ZnCl_2$ were found to have a 10:1 molar ratio of Zn^{2+} to protein (Table 3). Cadmium, in the original preparation, was measured at 1/50 000 of the zinc content. These protein samples were then dialyzed against $CdSO_4$-containing buffer in the absence of 2-mercaptoethanol and desalted through gel filtration before analysis by ICP-MS. As indicated in Table 3, Cd^{2+} substitution by direct dialysis resulted in 0.95 Cd^{2+} per subunit, with a residual of 0.3 Zn^{2+} equiv coordinated with the protein. All other metals were below the detection limits of the analysis. The resulting kinetic constants for the Cd^{2+}-containing enzyme, $K_m = 2.9 \pm 0.8$ μM, $k_{cat} = 0.21$ s^{-1} ($k_{cat}/K_m = 7 \times 10^4$ M^{-1} s^{-1}), indicate that the activity of the enzyme is comparable to that of zinc-containing PR-AMP cyclohydrolase, with k_{cat}/K_m affected by a 10-fold decrease.

Table 3: Summary of Metal Ion Analyses[a]

mol/subunit	Zn^{2+}	Cd^{2+}
M. thermoautotrophicum original preparation	10/10	-
M. thermoautotrophicum dialyzed against Cd^{2+}	0.3	0.95/0.97
M. vannielii His I	1/1	-

[a] Desalted using S-200 sepharose spin column. When two measurements were made, each result is reported.

DISCUSSION

The histidine biosynthetic pathway is highly conserved across a wide variety of organisms. While in some organisms *hisI* is a unique gene and in others a fusion with *hisE* creates a bifunctional enzyme, its amino acid sequence is highly conserved. The most highly conserved residues surround the surface cleft formed at the dimer interface that defines the putative catalytic site of the enzyme.

The steady-state kinetic and pH analyses of *M. thermoautotrophicum* HisI are consistent with the results from *M. vannielii* PR-AMP cyclohydrolase and indicate that the crystallized protein is enzymatically competent. The pH profile of k_{cat}/K_m is nearly bell-shaped, although the data are not adequate on the higher pH side to assess a second pK_a. On the low-pH side of the curve, the commitment factor occurs at the pK_a that is consistent with a cysteinyl side chain. Consistent with the suggestion that a protein side chain is being reflected in the pH dependence of the k_{cat}/K_m is the fact that the Cd^{2+}-substituted enzyme behaved in a similar manner. The substitution of cadmium for the active site zinc caused a greater decrease in the commitment factor at higher pH. However, the pH dependence of the protein reaction kinetics is essentially unchanged, with the pK_a of 7.55 for the zinc-containing protein versus 7.54 with cadmium.

Direct metal exchange experiments to replace the active site zinc with cadmium and subsequent kinetic analyses are consistent with the interpretation of the HisI structure depicting an active form of the enzyme. After desalting each ortholog using Sephacryl S-200 spin columns, the Zn^{2+} content of the *M. thermoautotrophicum* HisI was 10 times the amount determined for the ortholog from *M. vannielii* (Table 3). The amount of zinc associated with *M. thermoautotrophicum* HisI is consistent with the large number of Cd^{2+} ions observed in the crystal structure. Most of the metal-binding residues are conserved in *M. vannielii* HisI, yet analysis of this isoform consistently results in a 1:1 molar ratio of metal-to-protein. The larger number of Zn^{2+} associated with the enzyme preparation from *E. coli* may reflect a difference in the net charge of these two enzymes. Whereas *M. vannielii* has a total charge of −1 at pH 7, the *M. thermoautotrophicum* enzyme has a charge of −7, thus

Table 4: Kinetic Parameters of Native *M. Thermoautotrophicum* HisI (Zinc) Enzyme and *M. Thermoautotrophicum* HisI Dialyzed against Cd^{2+} (Cadmium)

	Zinc			Cadmium		
pH	k_{cat}	K_m	k_{cat}/K_m (mM^{-1} s^{-1})	k_{cat}	K_m	k_{cat}/K_m (mM^{-1} s^{-1})
6.5	1.7	112	0.0152	0.13	32.6	0.0040
7	8.7	73.4	0.1185	0.31	5	0.0620
7.5	7.5	33.6	0.2232	0.35	1.9	0.1842
8	6.4	13.6	0.4706	0.29	0.75	0.3867
8.5	9.9	20.4	0.4853	0.28	0.9	0.3111
9	7.4	19.8	0.3737	0.2	0.9	0.2222

requiring a larger number of counterions. Extensive dialysis of *M. thermoautotrophicum* HisI to replace zinc with cadmium resulted in a single molar equivalent of the replacement metal. Cadmium substitution does render the enzyme active, although not all of the zinc was displaced. The structure of the crystallized protein does provide a basis for evaluating the structural features of the enzyme active site. The catalytically unique features of the Cd^{2+}-substituted enzyme are reflected in the absolute changes in V_{max} and K_m values at the various pH values (Table 4). The relative impact of the metal substitution on these kinetic constants is compensatory, rendering the overall enzyme equal toward their substrate specificity at all pH values (Table 4, Figure 4).

The previous studies on the *M. vannielii* PR-AMP cyclohydrolase (*2*) demonstrated that catalysis requires both Zn^{2+} and Mg^{2+} ions. The Zn^{2+} is a high-affinity binding ligand, while the Mg^{2+} was shown to rapidly exchange. The mechanistic correlate for the cyclohydrolase reaction and the Zn^{2+}-dependent enzyme are the family of nucleoside/nucleotide hydrolases represented by adenosine deaminase and cytidine deaminase (*3*, *4*). The required stoichiometry of *M. vannielii* PR-AMP cyclohydrolase for Zn^{2+} is 1:1, and the three cysteine residues in the sequence motif $C^{93}(X)_{15}C^{109}H^{110}(X)_5C^{116}$ were suggested to be the Zn^{2+} ligands. Consistent with these observations is the three-dimensional structure of the *M. thermoautotrophicum* enzyme, which shows that the equivalent cysteine residues, Cys86, Cys102, and Cys109, form a metal binding site. Most interesting is the obligate dimeric feature of this structure which combines Cys86 from one monomer with two cysteines from the other monomer to complete the metal binding site. A solvent molecule completes the tetrahedral coordination of this bound metal ion. Mutations of the corresponding cysteine residues in the *M. vannielii* enzyme confirm that these residues form the Zn^{2+}-binding site and each of them is essential for enzymatic activity (D'Ordine et al., manuscript in preparation). Therefore, a fully competent enzyme requires dimerization to form the active site.

A requirement for free Mg^{2+} was demonstrated for the *M. vannielii* enzyme (*2*), and the model indicates co-binding of the substrates and metal. The triad of conserved aspartic acid residues in the cleft is a likely place for Mg^{2+} to bind. As expected for the Mg^{2+} ion, the Cd^{2+}(*2*) ion bound in this position in our structure is octahedrally coordinated. This metal ion neutralizes the adjacent negative charges of the carboxylate groups. The close proximity of this site to the putative Zn^{2+}-binding site is consistent with the requirement of Mg^{2+} for catalytic activity and is also consistent with the decreases in activity observed upon mutation of the *M. vannielii* equivalent of Asp87 (D'Ordine et al., manuscript in preparation).

The conserved sequence motif SR[S/T]RXX[L/I]WXKG-[E/A]TSG previously suggested to form a P-loop involved in Mg^{2+}/phosphate binding (*2*) corresponds to the sequence S^{60}TSRGKLWLKGESSG^{74} in *M. thermoautotrophicum*. Many of the highly conserved residues in HisI sequences are located in this motif. The three-dimensional structure reported here reveals that this motif forms one wall of the surface cleft. No metal-binding sites are localized to this loop and would indicate that the loop does not play the role of a classical Mg^{2+} and phosphate binding P-loop. Nonetheless, the conservation of these residues and their location imply that they play a crucial role in substrate binding.

To investigate possible substrate-binding roles of conserved residues in this motif, a model of 6-OH PR-AMP was docked into one of the two putative active site clefts of the HisI homodimer. 6-OH PR-AMP represents a tetrahedral intermediate formed by the attack of the Zn-activated water nucleophile to the purine C^6 atom of the PR-AMP substrate. This would be the mechanistic corollary to the tetrahedral intermediates formed in the purine/pyrimidine deaminases. This substrate has an approximate 2-fold symmetry, and two orientations of the elongated molecule are possible within the cleft of PR-AMP cyclohydrolase. The two binding modes were evaluated in detail. Flexible docking was achieved by Monte Carlo sampling of rotations around all six of the single bonds in the ligand, followed by energy minimization while constraining the 6-OH oxygen atom within the tetrahedral coordination geometry relative to the deduced Zn^{2+} location. The lowest energy model obtained for the HisI−transition state complex is shown in Figure 3D.

This model suggests plausible roles for the conserved residues in the HisI sequence. Specifically, the SR[S/T]RXX-[L/I]WXKG[E/A]TSG consensus motif contributes to the substrate binding. The side chains of Ser60 and Ser62 and the backbone nitrogen atom of Thr61 hydrogen-bond the adenosyl phosphate group, and side chain and backbone nitrogen atoms of Lys69, Gly70, Ser72, and Ser73 hydrogen-bond to the phosphoribosyl phosphate. The modeling suggests that Arg15, although not highly conserved among PR-AMP cyclohydrolases, provides additional stabilization of the adenosyl phosphate. The aromatic side chain of Trp67 interacts with both the adenine ring and the phosphoribosyl ribose ring. The deduced position of the Mg^{2+} ion suggests that it interacts with the adenosyl ribose rather than with the phosphate. The Asp87 carboxylate may also stabilize the transition state by interacting with the purine amino group at the tetrahedral C^6 atom.

D'Ordine et al. (*2*) noted the conservation of a histidine (His103 in *M. thermoautotrophicum*) and suggested that this residue may play a role in catalysis. In the crystal structure, this residue is involved in coordination of a Cd^{2+} ion bound between two symmetry-related molecules contributing to crystal contacts. This restraint likely influences the orientation and position of the histidine side chain relative to its conformation in solution. The model of the bound putative tetrahedral intermediate 6-OH PR-AMP provides the rationale for the role of His103. As seen in Figure 3D, rotation of the imidazole ring could allow a hydrogen bond to the

6-OH group and directly contact the scissile C^6-N^1 bond of the transition state (~3.4 Å). We could thus infer that His103 would be capable not only of positioning the Zn-activated water molecule in the ground state prior to transition state formation, but also of assisting in the conversion of the transition state toward product formation. Mutation of this histidine decreased the activity of the *M. vannielii* enzyme by approximately 3 orders of magnitude (D'Ordine et al., manuscript in preparation). A more detailed description of the proposed reaction mechanism will be presented in a subsequent paper (D'Ordine et al., manuscript in preparation).

In conclusion, the three-dimensional structure of HisI is consistent with the previous biochemical characterization of the enzyme. The proposed Zn^{2+}-binding site was identified to include three conserved cysteine residues as proposed previously, a likely binding site for the required Mg^{2+} ion has been localized, and the motif of conserved residues, although not a classical Mg^{2+}/phosphate-binding P-loop, is suggested by modeling of a reactive intermediate to be the substrate binding motif. The structure of the HisI catalytic site is consistent with a reaction mechanism similar to those of nucleoside deaminases.

REFERENCES

1. Singh, B. K. (1999) *Plant Amino Acids*, Marcel Dekker, Inc., New York.
2. D'Ordine, R. L., Klem, T. J., and Davisson, V. J. (1999) N1-(5′-phosphoribosyl)adenosine-5′-monophosphate cyclohydrolase: purification and characterization of a unique metalloenzyme, *Biochemistry 38*, 1537−1546.
3. Kinoshita, T., Nishio, N., Nakanishi, I., Sato, A., and Fujii, T. (2003) Structure of bovine adenosine deaminase complexed with 6-hydroxy-1,6-dihydropurine riboside, *Acta Crystallogr., Sect. D 59*, 299−303.
4. Johansson, E., Neuhard, J., Willemoes, M., and Larsen, S. (2004) Structural, kinetic, and mutational studies of the zinc ion environment in tetrameric cytidine deaminase, *Biochemistry 43*, 6020−6029.
5. Ireton, G. C., Black, M. E., and Stoddard, B. L. (2003) The 1.14 Å crystal structure of yeast cytosine deaminase: evolution of nucleotide salvage enzymes and implications for genetic chemotherapy, *Structure 11*, 961−972.
6. Fani, R., Mori, E., Tamburini, E., and Lazcano, A. (1998) Evolution of the structure and chromosomal distribution of histidine biosynthetic genes, *Origins Life Evol. Biosphere 28*, 555−570.
7. Beckler, G. S., and Reeve, J. N. (1986) Conservation of primary structure in the hisI gene of the archaebacterium, *Methanococcus vannielii*, the eubacterium *Escherichia coli*, and the eucaryote *Saccharomyces cerevisiae*, *Mol. Gen. Genet. 204*, 133−140.
8. Otwinowski, Z., and Minor, W. (1997) Processing of X-ray diffraction data collected in oscillation mode, in *Macromolecular Crystallography, part A* (Carter, C. W., Jr., and Sweet, R. M., Eds.) 276th ed., pp 307−326, Academic Press, New York.
9. Terwilliger, T. C. (2002) Automated structure solution, density modification and model building, *Acta Crystallogr., Sect. D 58*, 1937−1940.
10. Terwilliger, T. C., and Berendzen, J. (1999) Automated MAD and MIR structure solution, *Acta Crystallogr., Sect. D 55* (Pt 4), 849−861.
11. Jones, T. A., Zou, J.-Y., Cowan, S. W., and Kjeldgaard, M. (1991) Improved methods for building models in electron density maps and the location of errors in these models, *Acta Crystallogr., Sect. A 47*, 110−119.
12. Brunger, A. T., Adams, P. D., Clore, G. M., DeLano, W. L., Gros, P., Grosse-Kunstleve, R. W., Jiang, J. S., Kuszewski, J., Nilges, M., Pannu, N. S., Read, R. J., Rice, L. M., Simonson, T., and Warren, G. L. (1998) Crystallography & NMR system: A new software suite for macromolecular structure determination, *Acta Crystallogr., Sect. D. 54*, 905−921.
13. Laskowski, R. A., MacArthur, M. W., Moss, D. S., and Thornton, J. M. (1993) PROCHECK: a program to check the stereochemical quality of protein structures, *J. Appl. Crystallogr. 26*, 283−291.
14. Chowdhury, S. F., Sivaraman, J., Wang, J., Devanathan, G., Lachance, P., Qi, H., Menard, R., Lefebvre, J., Konishi, Y., Cygler, M., Sulea, T., and Purisima, E. O. (2002) Design of noncovalent inhibitors of human cathepsin L. From the 96-residue proregion to optimized tripeptides, *J. Med. Chem. 45*, 5321−5329.
15. Lin, L. Y., Sulea, T., Szittner, R., Vassilyev, V., Purisima, E. O., and Meighen, E. A. (2001) Modeling of the bacterial luciferase-flavin mononucleotide complex combining flexible docking with structure−activity data, *Protein Sci. 10*, 1563−1571.
16. Li, Z., and Scheraga, H. A. (1987) Monte Carlo-minimization approach to the multiple-minima problem in protein folding, *Proc. Natl. Acad. Sci. U.S.A. 84*, 6611−6615.
17. Cornell, W. D., Cieplak, P., Bayly, C. I., Gould, I. R., Merz, K. M., Ferguson, D. M., Spellmeyer, D. C., Fox, T., Caldwell, J. W., and Kollman, P. A. (1995) A second generation force field for the simulation of proteins, nucleic acids, and organic molecules., *J. Am. Chem. Soc. 117*, 5179−5197.
18. Wang, J., Wolf, R. M., Caldwell, J. W., Kollman, P. A., and Case, D. A. (2004) Development and testing of a general amber force field, *J. Comput. Chem. 25*, 1157−1174.
19. Cornell, W. D., Cieplak, P., Bayly, C. I., and Kollman, P. A. (1993) Application of RESP chrages to calculate conformational energies, hydrogen bond energies, and free energies of solvation, *J. Am. Chem. Soc. 115*, 9620−9631.
20. Pang, Y. P., Xu, K., Yazal, J. E., and Prendergas, F. G. (2000) Successful molecular dynamics simulation of the zinc-bound farnesyltransferase using the cationic dummy atom approach, *Protein Sci. 9*, 1857−1865.
21. Auld, D. S. (1988) Methods for metal substitution, *Methods Enzymol. 158*, 71−79.
22. Barton, G. J. (1993) ALSCRIPT a tool to format multiple sequence alignments, *Protein Eng. 6*, 37−40.
23. Gibbons, C., Montgomery, M. G., Leslie, A. G., and Walker, J. E. (2000) The structure of the central stalk in bovine F(1)-ATPase at 2.4 Å resolution, *Nat. Struct. Biol. 7*, 1055−1061.
24. Fedorov, R., Meshcheryakov, V., Gongadze, G., Fomenkova, N., Nevskaya, N., Selmer, M., Laurberg, M., Kristensen, O., Al-Karadaghi, S., Liljas, A., Garber, M., and Nikonov, S. (2001) Structure of ribosomal protein TL5 complexed with RNA provides new insights into the CTC family of stress proteins, *Acta Crystallogr., Sect. D 57*, 968−976.
25. Lu, M., and Steitz, T. A. (2000) Structure of *Escherichia coli* ribosomal protein L25 complexed with a 5S rRNA fragment at 1.8-Å resolution, *Proc. Natl. Acad. Sci. U.S.A 97*, 2023−2028.
26. Zvereva, M. E., Shpanchenko, O. V., Nierhaus, K., and Dontsova, O. A. (2000) Ribosomal protein TL5 of *T. thermophilus* is incorporated in the *E. coli* 50S ribosomal subunit, *Dokl. Biochem. 374*, 199−201.

BI050472W